Optics and Lasers in Engineering 84 (2016) 96–104

Contents lists available at ScienceDirect

Optics and Lasers in Engineering

journal homepage: www.elsevier.com/locate/optlaseng

An omnidirectional 3D sensor with line laser scanning

Jing Xu [a,b,*], Bingtuan Gao [c], Chuande Liu [c], Peng Wang [a,b], Shuanglei Gao [a,b]

[a] State Key Laboratory of Tribology, Mechanical Engineering, Tsinghua University, Beijing 100084, China
[b] State Key Laboratory of Robotics, Shenyang Institute of Automation, Chinese Academy of Sciences, Shenyang 110016, China
[c] School of Electrical Engineering, Southeast University, Nanjing 210096, China

ARTICLE INFO

Article history:
Received 16 November 2014
Received in revised form
15 February 2016
Accepted 5 April 2016
Available online 22 April 2016

Keywords:
Omnidirectional vision
Laser line scanning
Calibration

ABSTRACT

An active omnidirectional vision owns the advantages of the wide field of view (FOV) imaging, resulting in an entire 3D environment scene, which is promising in the field of robot navigation. However, the existing omnidirectional vision sensors based on line laser can measure points only located on the optical plane of the line laser beam, resulting in the low-resolution reconstruction. Whereas, to improve resolution, some other omnidirectional vision sensors with the capability of projecting 2D encode pattern from projector and curved mirror. However, the astigmatism property of curve mirror causes the low-accuracy reconstruction. To solve the above problems, a rotating polygon scanning mirror is used to scan the object in the vertical direction so that an entire profile of the observed scene can be obtained at high accuracy, without of astigmatism phenomenon. Then, the proposed method is calibrated by a conventional 2D checkerboard plate. The experimental results show that the measurement error of the 3D omnidirectional sensor is approximately 1 mm. Moreover, the reconstruction of objects with different shapes based on the developed sensor is also verified.

1. Introduction

In the field of mobile robots, typically, vision is used in perception and navigation sensing to build the 3D scene, which is expressed by a 3D point cloud, because vision possesses the following advantages: rich information, high frequency, and low cost. Based on whether additional illumination is projected onto an observed target, vision can be categorized as passive vision and active vision.

Passive vision, in which the target does not receive additional illumination, is widely utilized because of its simplicity and compactness. Furthermore, according to the number of viewpoints (input images), passive vision can be further categorized as monocular vision and stereo vision. In monocular vision, the target distance is measured by using the depth of field [1]. In stereo vision, the 3D profile is obtained by using triangulation of multiview images [2]. The key challenge in stereo vision is correspondence matching, which depends on scene properties such as texture, illumination, and reflectance.

To improve sensing reliability, active vision can label an artificial texture onto the surface of a measured object by projecting encoded illumination; thus, correct correspondence matching can be obtained, regardless of the variant environment. Therefore, active vision has certain advantages, such as high resolution, high accuracy, high speed, simple structure, and high reliability. Hence, active vision is being increasingly applied to short-distance target sensing in the field of mobile robots.

The earliest cheap, commercial active vision sensor can be traced back to Microsoft Kinect, which is capable of quickly measuring the 3D profile and color [3]. Then, an increasing number of research groups studied various applications of perception and navigation with Kinect in the field of mobile robots, and a large number of relevant studies have been published [4–6]. However, the significant drawback of Kinect is its limited field of view (FOV), which is approximately 60° and 45° in the horizontal and vertical directions, respectively. Therefore, the observed features are displayed in the sensor for only a short period of time when the mobile robot moves continuously. For a mobile robot, the feature viewing time is too short to avoid an obstacle in the complex environment without the entire 3D scene.

For a mobile robot, the 3D sensor can help build an entire omnidirectional 3D scene. Therefore, omnidirectional vision is preferred due to the advantages of its wide FOV. More importantly, omnidirectional vision can provide a continuous omnidirectional 3D scene, which is significantly helpful to the mobile robot in a narrow space or under partial occlusion [7]. Thus, such a sensor is a promising one that enables the mobile robot to perceive an unknown, complicated, and dynamic environment in all directions in real time.

* Corresponding author at: State Key Laboratory of Tribology, Mechanical Engineering, Tsinghua University, Beijing 100084, China.
E-mail address: jingxu@tsinghua.edu.cn (J. Xu).

http://dx.doi.org/10.1016/j.optlaseng.2016.04.001
0143-8166/

To achieve omnidirectional vision, one approach is the use of multiple sets of cameras; however, this method results in blind spots, measured point cloud alignment, and cumbersome measurement procedures [8]. An alternative approach is the use of a catadioptric camera; it consists of a normal perspective lens and a curved mirror (such as hyperbola, parabola, or cone mirror), which can project the omnidirectional FOV scene onto a camera in real time [9]. Hence, this second approach is widely used in the field of mobile robots [10].

Similar to other traditional passive vision systems, the biggest challenge in 3D omnidirectional vision sensors is correspondence matching. To solve this problem, an active 3D omnidirectional vision has been proposed. Four sets of line lasers are used to generate an optical plane around the sensor, whereas the catadioptric camera captures the ambient scene with a distorted laser image to obtain the coordinates. A system calibration method is described in [11,12]. Based on this approach, a single laser installed with a conical mirror is also used to generate an optical plane [13]. Additionally, a similar 3D omnidirectional measurement system has been presented in [14,15]. However, these systems can measure the 3D point cloud in only one optical plane. In general, the low resolution of the measured point cloud is not sufficient to obtain the entire and detailed profile of the object [16].

A 3D laser-based omnidirectional sensor has been developed to obtain high resolution; however, its mechanical structure is complicated. Similarly, multiple sets of projectors are used to project different encoded patterns onto the object [17]; then, a catadioptric camera is used to capture the distorted patterns to significantly improve the spatial resolution of the measured point cloud. However, some blind spots continued to exist, and fast measurements could not be achieved. To address these challenges, a fast 3D omnidirectional sensor with a balance between accuracy and resolution was developed in our previous study [18]. It contains an LED projector and a camera. The encoded pattern of the projector is projected onto the surrounding scene through a hyperbolic mirror; then, the camera installed with a hyperbolic mirror captures distorted patterns to quickly obtain the 3D point cloud. However, the inevitable astigmatism property of a curved mirror will result in an inaccurate 3D reconstruction. In recent years, the development of a low-cost, high-accuracy, high-resolution 3D omnidirectional sensor that can offer a real-time 3D omnidirectional scene has become one of the most popular research topics in the field of mobile robots.

To address the above limitations, in this paper, we present a 3D omnidirectional sensor with high accuracy and high resolution. The proposed sensor can build the entire surrounding 3D omnidirectional scene form several consecutive images obtained by using a rotated optical plane; this approach eliminates blind spots and astigmatism and is inspired by the laser scanning technique. A significant feature is that the reconstruction speed depends only on the frame rate of the camera, i.e., the method can achieve real-time reconstruction of the scene.

The remainder of the paper is structured as follows: Section 2 describes the principle and geometric configuration of the proposed 3D sensor; Section 3 presents the systematic calibration method; the mechanical design and sensor performance verification are discussed in Section 4; Section 5 states the conclusion of our study.

2. Sensor principle

2.1. System description

The proposed 3D omnidirectional sensor contains a line laser transmitter module and a line laser receiver module as shown in Fig. 1. The line laser transmitter module consists of a rotating polygon scanning mirror and two line lasers. The fan angle of each line laser beam is 180°, which is implemented by a semicircle laser beam reflected by a cone mirror as shown in Fig. 2. Conventionally, the laser beam is directly focused onto the object; therefore, we can obtain the 3D coordinates of only those points that are located at the intersection of the object surface and the optical plane of the line laser beam. However, the conventional method can obtain only a low-resolution, coplanar, and local point cloud of the object,

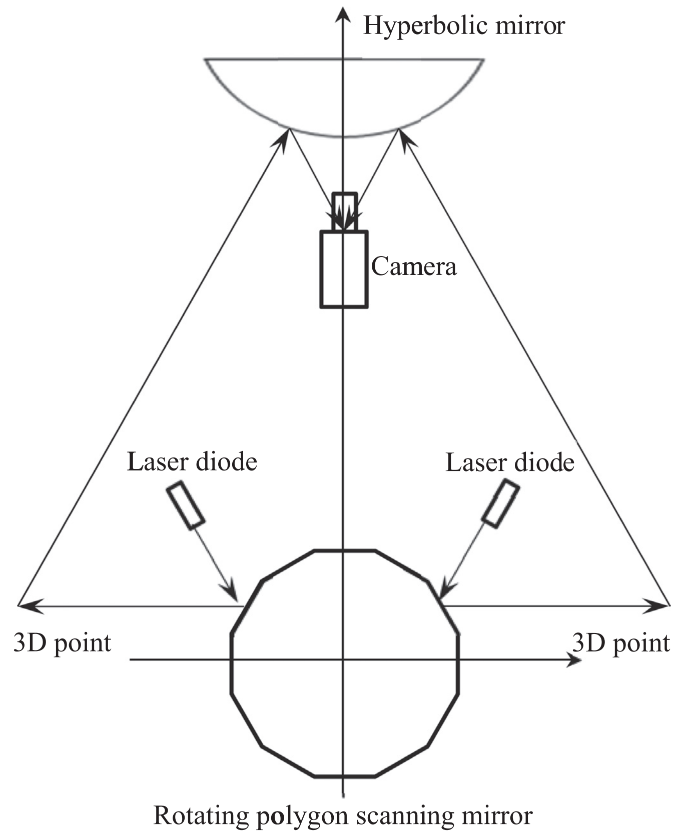

Fig. 1. System architecture.

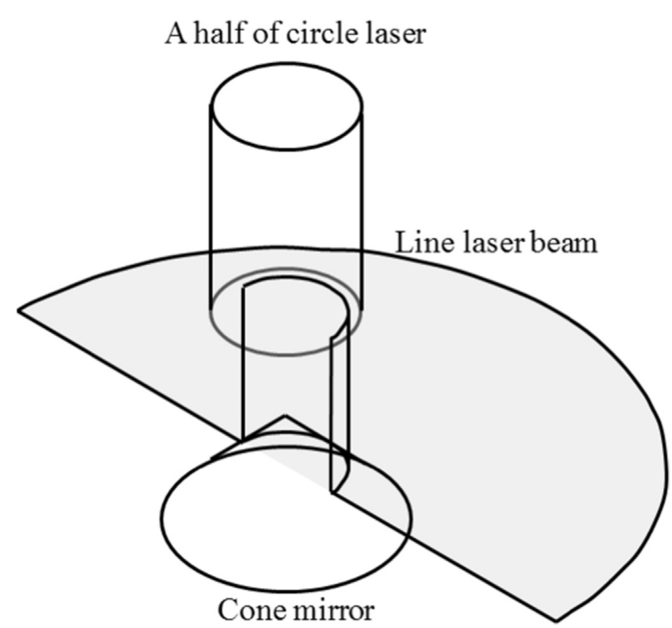

Fig. 2. Line laser beam with a fan angle of 180°.

cannot obtain the entire profile of the object.

Inspired by the laser scanning technique, our study aims to enable the optical plane of the linear laser beam to scan along the vertical direction. For this purpose, the line laser beam with a fan angle of 180° is designed to focus onto a rotating polygon scanning mirror instead of the observed object, as shown in Fig. 1; this design enables the optical plane of the reflected line laser beam to scan the object at a step of a certain angle from top to bottom. In this case, we can obtain consecutive slices of the point cloud of the object surface; thus, an entire point cloud of the object surface can be generated by merging consecutive slices of the point cloud. A smaller interval angle of the rotating polygon scanning mirror yields a 3D point cloud with higher resolution. It should be noted that a rotating polygon scanning mirror is easy to control and could achieve high angular accuracy with a high-resolution encoder. The scanning mirror could be synchronized with the camera exposure for automatic measurement; thus, we could obtain the location of each optical plane of the line laser beam in the world space.

The line laser receiver module is a catadioptric camera, which consists of an imaging sensor (including a CCD camera and a perspective lens) and a hyperbolic mirror. The hyperbolic mirror, is used to image a 360° cylindrical FOV scene in the CCD camera. Then, each pixel of the line laser beam in the camera could be transformed to an optical line in the world space. Hence, the measured point is located at the intersection of the optical plane of the line laser beam and the optical line to the camera.

2.2. Line laser installation

For the rotating polygonal scanning mirror, the maximum scanning angle of the reflected light depends on the number of sides of the regular polygon. When the number of sides is n, the central angle (the angle between the segments of the circle center and any two adjacent vertices of the polygon) of each side of the polygon is $360°/n$, and the scanning angle is $720°/n$. Assume that a designed 3D sensor requires the degree of the pitch angle to be 60° and symmetrical with respect to the horizontal direction, i.e., the angle with respect to the horizontal direction ranges from −30° to 30°. Then, the required number of sides of the regular polygon is 12.

The scanning range of −30° to 30° in the vertical direction determines the position and orientation of the line laser. The coordinate system of the rotating polygonal scanning mirror is defined as shown in Fig. 3. The radius of the circumscribed circle of the rotating polygonal scanning mirror is R, and the central angle of a circle chord 13 is 2θ, where $\theta = 15°$. In this case, the reflection angle of the horizontal reflected light is 2θ. The chordal endpoint 1 coordinates are $(R\cos\theta, R\sin\theta)$, the chordal endpoint 2 coordinates are $(R\cos 3\theta, R\sin 3\theta)$, and the chordal midpoint 3 coordinates are $(R\cos\theta\cos 2\theta, R\cos\theta\sin 2\theta)$. According to the reflection law, the angle of reflection is equal to the angle of incidence; hence, the angle between the incident light and x-axis is 4θ.

Thus, the line laser diode must be installed at an angle of 4θ with respect to the horizontal direction, and the light ray passes through chordal midpoint 3, i.e., the equation for the incident light from the line laser beam is:

$$z - R\cos\theta\sin 2\theta = \tan 4\theta(x - R\cos\theta\cos 2\theta) \tag{1}$$

2.3. 3D reconstruction

A 3D point in space is reconstructed with the optical plane of the line laser beam and the optical line of the corresponding camera pixel. Therefore, first, we specify the equations of the optical plane and the optical line; second, we determine the intersection of the optical plane and the optical line to obtain the 3D point.

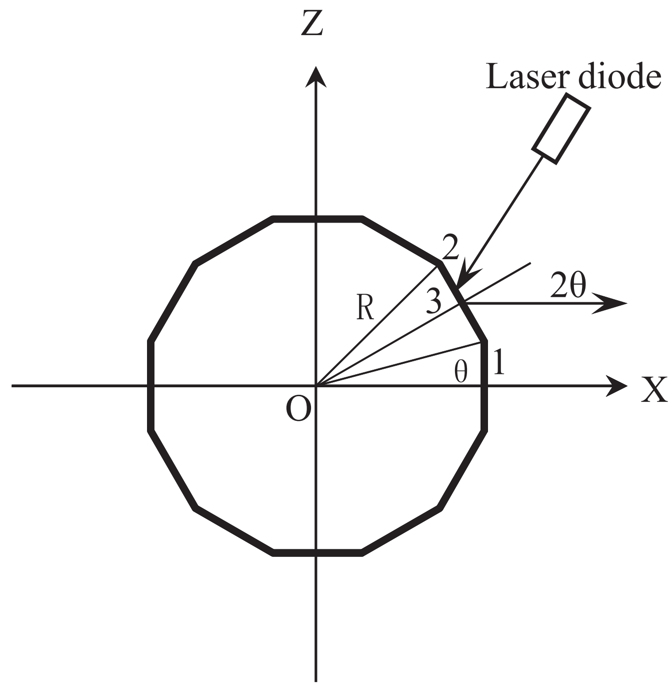

Fig. 3. Laser diode installation.

2.3.1. Geometry of line laser transmitter

This section aims to obtain the optical plane of the line laser beam with respect to the rotation angle of the scanning mirror.

Without loss of generality, the initial position and the coordinate frame of the line laser transmitter are shown in Fig. 4. When the polygonal scanning mirror rotates counterclockwise by $\alpha (0\alpha < 2\theta)$, the rotation angle of the reflected light will be 2α. When the rotating polygonal scanning mirror rotates by $\alpha = 2\theta$, the system reverts to its initial state, and the next cycle will repeat as shown in Fig. 4. If the rotating polygonal scanning mirror continues to rotate, repeated scans from the left to right side of Fig. 4 can be obtained. The rotating polygonal scanning mirror can easily achieve a large scanning angle, high scanning speed, and high resolution, and it eliminated astigmatism.

In Fig. 4, the coordinates of chordal endpoint 1 are $(R\cos\alpha, R\sin\alpha)$, and the coordinates of chordal endpoint 2 are $(R\cos(2\theta+\alpha), R\sin(2\theta+\alpha))$. The equation of chord 12 is:

$$z - R\sin\alpha = -\frac{\cos(\theta+\alpha)}{\sin(\theta+\alpha)}(x - R\cos\alpha) \tag{2}$$

Thus, the intersection of chord 12 and the incident light is:

$$\begin{cases} x_\alpha = R\dfrac{2\cos 3\theta + 2\cos 5\theta + \cos\alpha}{4\cos(\alpha - 3\theta)} \\ \quad + R\dfrac{\cos(\alpha - 2\theta) - \cos(\alpha + 2\theta) - \cos(\alpha + 4\theta)}{4\cos(\alpha - 3\theta)} \\ z_\alpha = R\dfrac{2\sin\alpha\cos^4\theta - 2\sin\alpha\cos^2\theta + 4\sin\theta\cos^2\theta}{2\sin^2\dfrac{\alpha - 3\theta}{2} - 1} \\ \quad + R\dfrac{2\cos\alpha\sin\theta\cos^3\theta - 8\sin\theta\cos^4\theta}{2\sin^2\dfrac{\alpha - 3\theta}{2} - 1} \end{cases} \tag{3}$$

Then, the equation of the optical plane of the reflected line laser beam is:

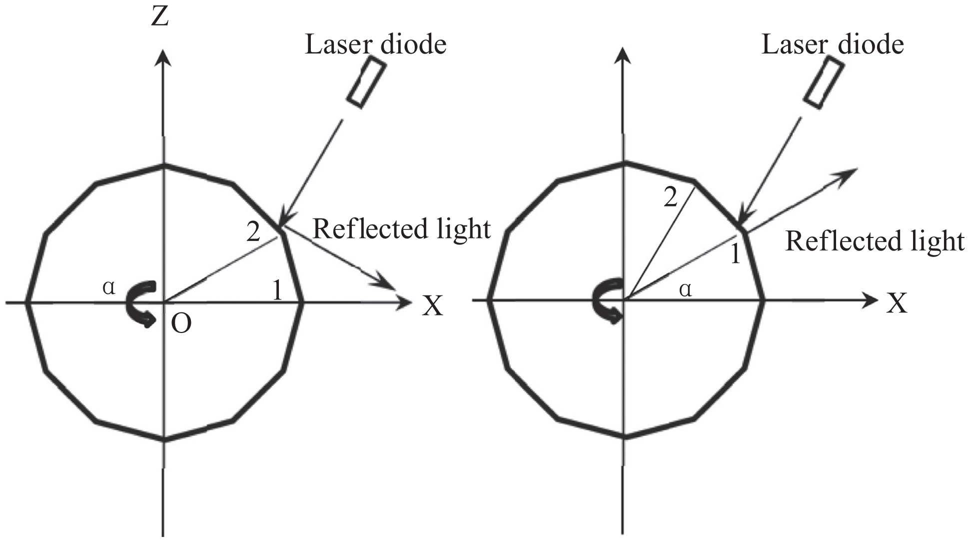

Fig. 4. Scanning mirror.

$$z - z_\alpha = \tan(2\alpha - 2\theta)(x - x_\alpha) \quad (4)$$

which can be further transformed into the slope and intercept form:

$$z = \tan(2\alpha - 2\theta)x + b \quad (5)$$

where b is the intersection. Given a mirror rotation angle α, we can obtain the equation of the optical plane of the reflected line laser beam.

It is obvious that intersection b is non-constant during the rotation process, i.e., the intercept of the optical plane of the reflected line laser beam along z-axis is nonlinear as the mirror rotates. To simplify the computation, a lookup table (LUT) of the z-axis intercept b with respect to the rotation angle can be obtained offline, as detailed in Table 1 and illustrated in Fig. 5.

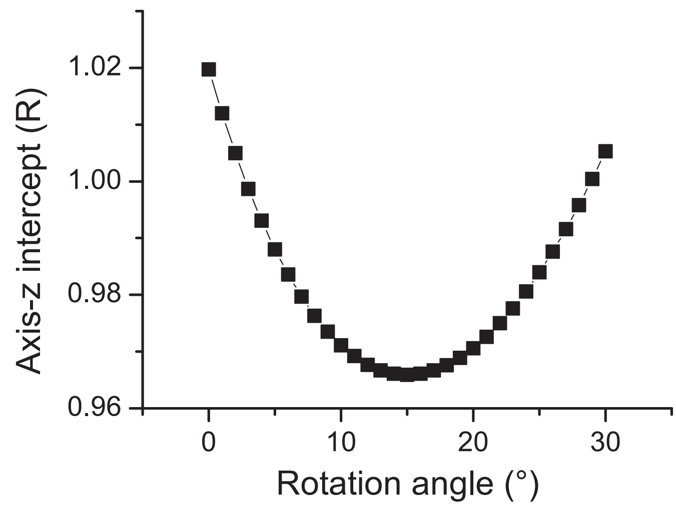

Fig. 5. Axis-z intercept.

2.3.2. Geometry of line laser receiver

This section aims to obtain the optical line with respect to the camera pixel.

The characteristic of a hyperbolic mirror is that any incident light ray passing through one focus of the mirror will be reflected by the mirror and pass through another focus of the mirror, as shown in Fig. 6. Without loss of generality, one focus of the hyperbolic mirror is located at $(0, 0, 0)$, and another focus is at $(0, 0, 2c)$. If the optical center of a CCD camera is identical to the focus of the hyperbolic mirror [19], the system has a single viewpoint, as shown in Fig. 6. The hyperbolic mirror can be represented by:

Table 1
The relationship between intersection of angle and intercept.

Serial number	α	$b(R)$	Serial number	α	$b(R)$
1	0	1.0197	17	16	0.9661
2	1	1.0120	18	17	0.9667
3	2	1.0050	19	18	0.9676
4	3	0.9987	20	19	0.9689
5	4	0.9931	21	20	0.9706
6	5	0.9880	22	21	0.9726
7	6	0.9836	23	22	0.9750
8	7	0.9797	24	23	0.9776
9	8	0.9763	25	24	0.9806
10	9	0.9735	26	25	0.9840
11	10	0.9711	27	26	0.9876
12	11	0.9692	28	27	0.9916
13	12	0.9677	29	28	0.9958
14	13	0.9667	30	29	1.0004
15	14	0.9661	31	30	1.0053
16	15	0.9659			

$$\frac{(z-c)^2}{a^2} - \frac{x^2+y^2}{b^2} = 1 \quad (6)$$

where $c = \sqrt{a^2 + b^2}$.

To simplify the notation, the coordinate frame of the line laser receiver is assumed to coincide with the coordinate frame of the camera. If a pixel Q is set to be (u,v) in the camera frame, the angle β between the optical axes and the reflected light ray $\overrightarrow{MO}$ to the camera can be represented by:

$$\beta = \arctan\frac{l}{f} \quad (7)$$

where $l = \sqrt{u^2 + v^2}$, and f is the focal length of the lens.

According to the property of a hyperbolic mirror,

$$|FM| = |OM| - 2a \quad (8)$$

Further, the geometrical relation in Fig. 6 is as follows:

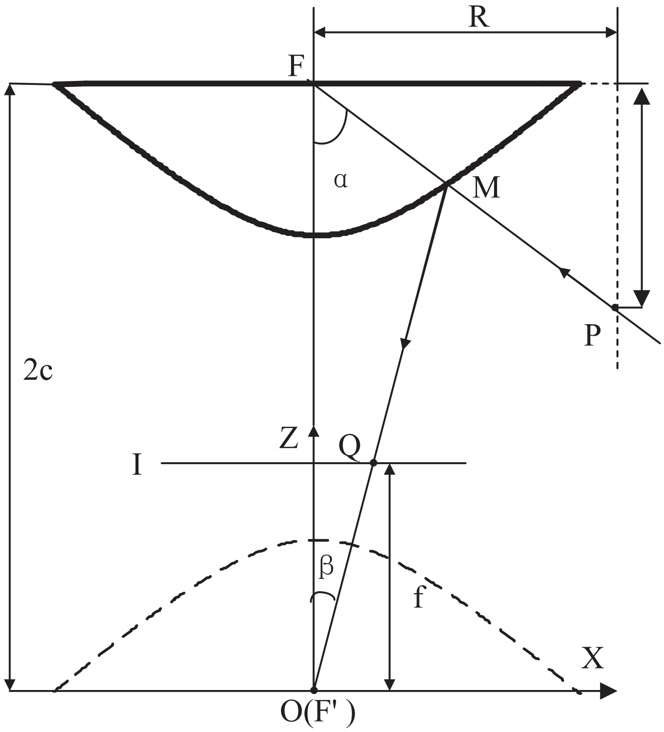

Fig. 6. Optical path of pixel Q.

$$\begin{cases} OM\cdot\sin\beta = (OM - 2a)\sin\alpha \\ OM\cdot\cos\beta + (OM - 2a)\cos\alpha = 2c \end{cases} \tag{9}$$

where α is the angle between the optical axes and the incoming light ray to the hyperbolic mirror. Then, we obtain:

$$OM = \frac{c^2 - a^2}{c\cdot\cos\beta - a} \tag{10}$$

To determine the incident optical line $\overrightarrow{MF}$, first, we obtain the point M on the hyperbolic mirror surface in the camera coordinate frame:

$$\begin{cases} x_M = \dfrac{u\left(c^2 - a^2\right)\sin\beta}{l(c\cdot\cos\beta - a)} \\ y_M = \dfrac{v\left(c^2 - a^2\right)\sin\beta}{l(c\cdot\cos\beta - a)} \\ z_M = \dfrac{\left(c^2 - a^2\right)\cos\beta}{c\cdot\cos\beta - a} \end{cases} \tag{11}$$

Subsequently, the incident optical line $\overrightarrow{MF}$ in the camera coordinate frame is subject to:

$$\frac{x}{x_M} = \frac{y}{y_M} = \frac{z - 2c}{z_M - 2c} \tag{12}$$

The incident optical line $\overrightarrow{MF}$ can be further rewritten as:

$$\begin{cases} x = x_M i \\ y = y_M i \\ z = 2c + (z_M - 2c)i \end{cases} \tag{13}$$

where i is a coefficient. Additionally, the incident optical line $\overrightarrow{MF}$ can also be represented in a polynomial form [20].

2.3.3. *Coordinates of world point*

The coordinate systems of the line laser transmitter and receiver are aligned coaxially. To simplify the notation, the world coordinate frame is assumed to coincide with the line laser receiver coordinate system, which is also the camera coordinate system. The origin of the line laser transmitter coordinate system is located at $(0, 0, -h)$ in the world coordinate frame. Hence, the optical plane of the line laser beam, Eq. (5), in the world coordinate frame can be rewritten as:

$$z = \tan(2\alpha - 2\theta)x + b - h \tag{14}$$

Thus, the 3D point is the intersection of Eqs. (13) and (14).

$$\begin{cases} x_P = \dfrac{x_M(b - h - 2c)}{z_M - 2c - \tan(2\alpha - 2\theta)x_M} \\ y_P = \dfrac{y_M(b - h - 2c)}{z_M - 2c - \tan(2\alpha - 2\theta)x_M} \\ z_P = 2c + \dfrac{(z_M - 2c)(b - h - 2c)}{z_M - 2c - \tan(2\alpha - 2\theta)x_M} \end{cases} \tag{15}$$

Thus, we have achieved the 3D reconstruction by using the proposed multidirectional 3D sensor.

3. Calibration

The developed 3D omnidirectional sensor is expected to accurately construct the ambient scene. Prior to application, the calibration of the sensor is a critical step. This section describes the calibration of the sensor. The calibration process consists of two steps:

(1) calibration of the line laser receiver, i.e., the parameter of the optical line with respect to the corresponding pixel in the world coordinate system;
(2) calibration of the line laser transmitter, i.e., the parameter of the optical plane with respect to the rotation angle in the world coordinate system.

Line laser receiver calibration can be easily achieved by using a 2D checkerboard plate [20]. After calibration, an optical line in the 3D space can be obtained for every pixel in the camera. Therefore, this paper focuses on a method for calibrating the line laser transmitter.

To calibrate an optical plane, at least three non-collinear points are required. However, an optical plane projected onto the 2D checkerboard plate generates a straight line, which is not sufficient to identify an optical plane. Hence, one approach is the movement of one checkerboard plate to another location to generate two straight lines; an alternative solution is the establishment of two perpendicular checkerboard plates to generate two cross straight

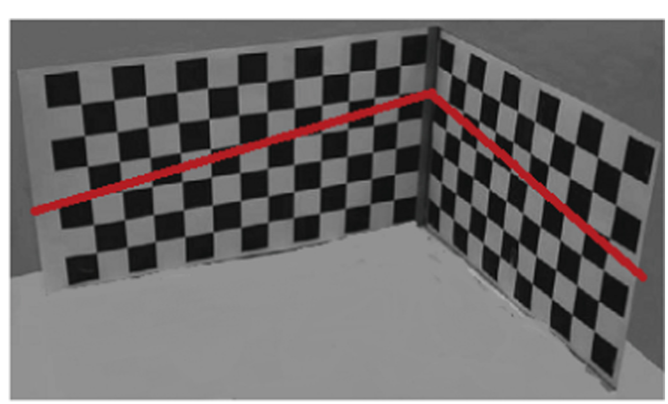

Fig. 7. Calibration gauge of 3D sensor.

lines simultaneously. In this paper, the latter approach is employed in the calibration process.

As shown in Fig. 7, the optical plane of the line laser beam is projected onto the two perpendicular checkerboard plates. The homography matrix of the two calibration plates can be obtained separately by using known camera parameters. If the ridge of the laser line on the image is extracted, the spatial coordinates of the laser line on two calibration plates can be obtained with the homography matrix; then, the equation of the optical plane of the line laser beam can be fitted.

It should be noted that the laser beam on the checkerboard plate has a certain width. To improve the calibration and measurement accuracy, the ridge of the laser line beam must be extracted.

First, the laser line beam should be extracted from the image by using a threshold, i.e., the laser line beam is brighter than the setting threshold.

Next, the image is scanned line by line, perpendicular to the laser line beam. Typically, the brightness of several pixels is greater than the setting threshold; then, the intensity centroid is used to determine the ridge of the laser beam at a sub-pixel level by

$$y = \frac{\sum_{i=1}^{n} Gray_i \cdot y_i}{\sum_{i=1}^{n} Gray_i} \tag{16}$$

where n is the number of pixels greater than the setting threshold, y_i denotes the longitudinal coordinates, and $Gray_i$ represents the intensity of the pixel point (x, y_i).

4. Experimental verification

4.1. Experimental prototype

The proposed 3D omnidirectional sensor consists of two line lasers, a scanning mirror, a hyperbolic mirror, a perspective camera, some mechanical structures, and connections. To cover a 360° ambient environment without blind spots, two line laser diodes are placed, one on either side of the scanning mirror, i.e., one line laser can cover a 180° ambient environment. As shown in Fig. 8, the scanning mirror and laser diodes are very compact, and the two laser diodes must be aligned symmetrically around the rotation axis of the scanning mirror.

Furthermore, to guarantee that the camera has a maximum FOV, the optical axis of the camera and the rotation axis of the scanning mirror should intersect (as shown in Fig. 8). The camera support structure can be adjusted slightly to place the camera at a suitable position and orientation. The distance between the optical plane of the line laser beam and the camera is adjustable in our system to meet the various measurement requirements. The camera is supported by a single pole, and the support pole is on the rotation axis of the scanning mirror; thus, the camera FOV is maximized.

As shown in Fig. 9, the camera is connected firmly to the housing of the hyperbolic mirror with $a^2 = 1248.2060$ and $b^2 = 351.7940$. To meet the requirement of a single viewpoint of a hyperbolic mirror catadioptric camera system, the optical centers of camera lens and hyperbolic mirror must be coincident.

To ensure a clear image for automatic measurement, the scanning mirror and camera exposure must be synchronized. Therefore, the camera operates in the trigger mode; the scanning mirror sends a trigger signal to the camera at a certain angle, and then, the camera captures the scene. In this case, a slice of the 3D profile is obtained. The entire profile is obtained by merging consecutive slices of the 3D profile. It should be noted that the

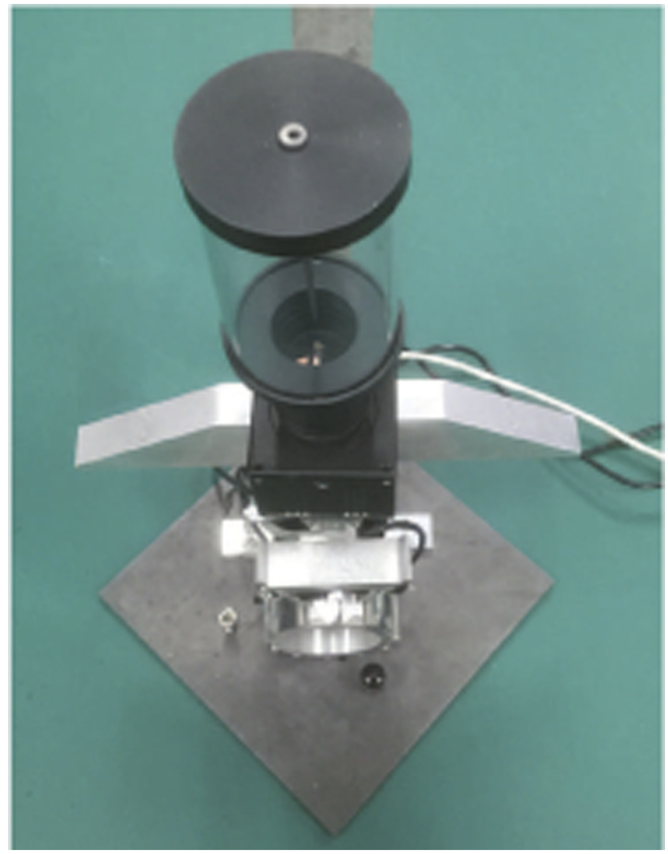

Fig. 8. Configuration of the 3D omnidirectional sensor.

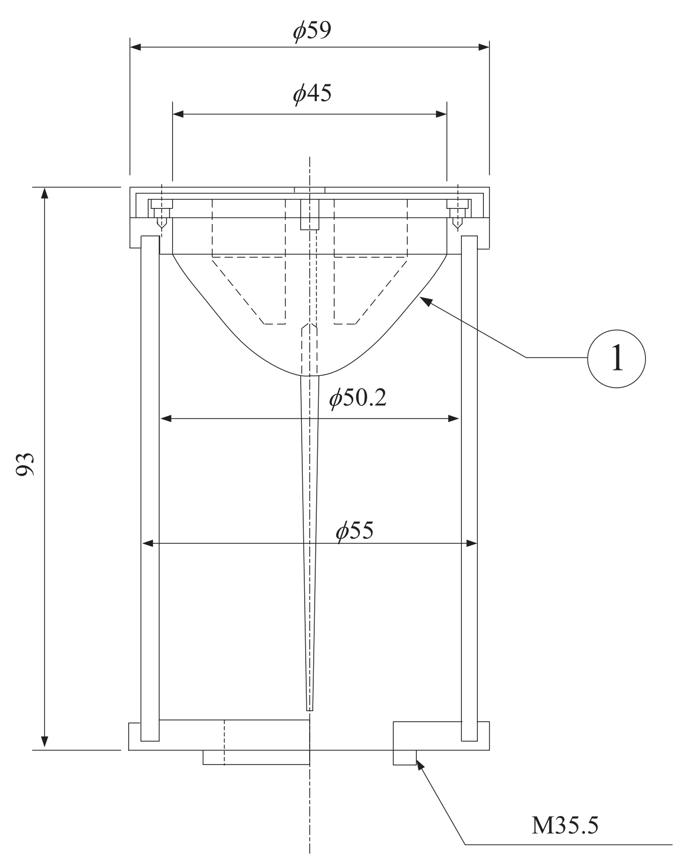

Fig. 9. Hyperboloid mirror and glass housing.

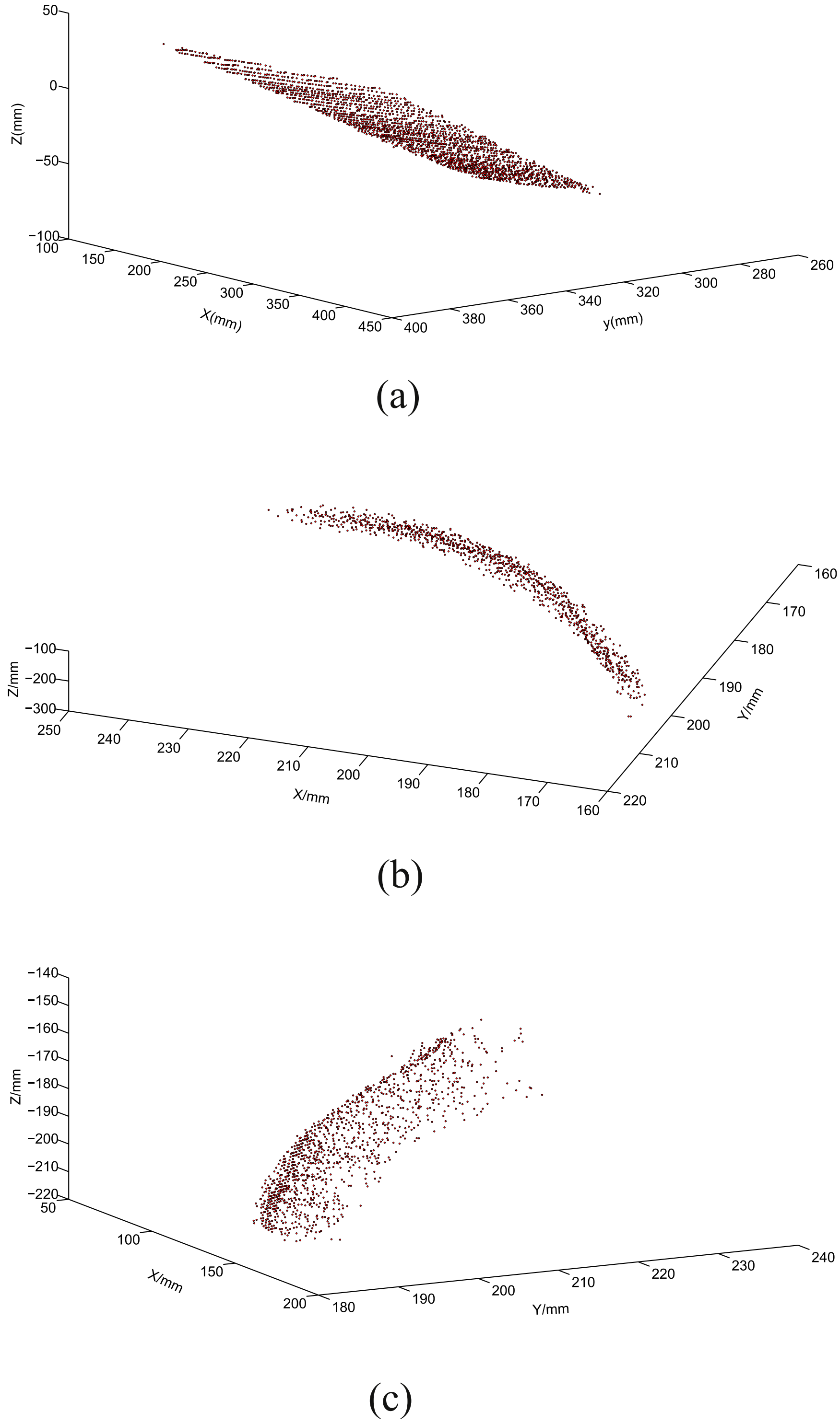

Fig. 10. The measured point clouds: (a) plane, (b) cylinder, and (c) sphere.

sensor is expected to be fixed during merging; otherwise, the displacement of the point cloud for each frame must be compensated after the robot moves.

To test the measurement accuracy of the proposed 3D omnidirectional sensor, three different shapes from simple geometry to complicated geometry, including a plane, a cylinder, and a sphere, are measured in this study. The measured point clouds of the measured plane, cylinder, and sphere after denoising are plotted in Fig. 10(a), (b), and (c), respectively. Then, a quantitative analysis of the system measurement accuracy can be obtained based on the measurement results from simple geometry to complicated geometry. For the plane, cylinder, and sphere after denoising, the mean measurement errors are approximately 0.21 mm, 0.24 mm, and -0.17 mm, respectively, whereas the standard deviations are approximately 0.49 mm, 0.93 mm, and 1.24 mm, respectively. Intuitively, the proposed 3D omnidirectional sensor has very high

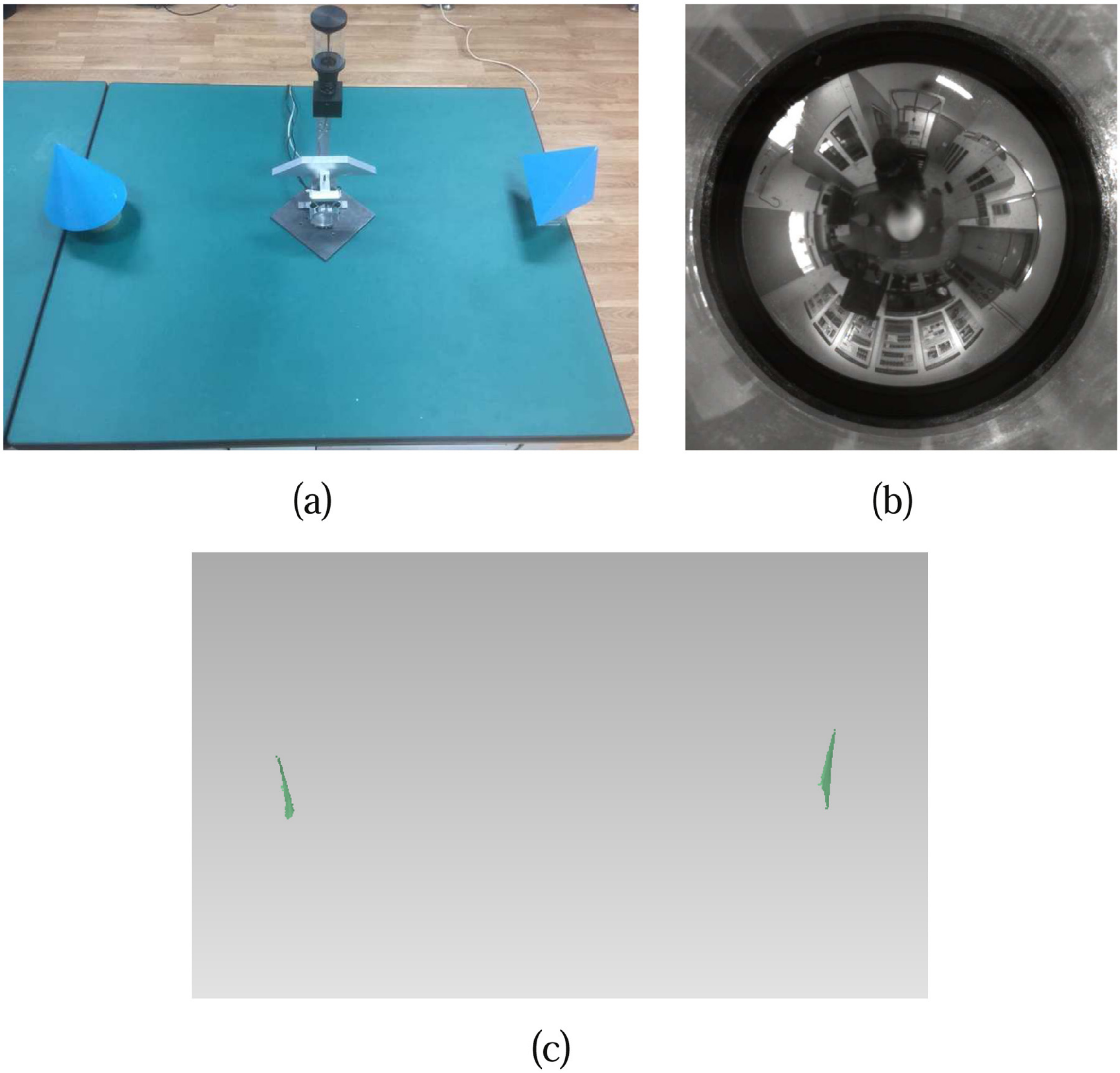

Fig. 11. 3D reconstruction: (a) scene, (b) captured image, and (c) point cloud.

measurement accuracy. Furthermore, the results show that as the complexity of the shape increases, the measurement accuracy decreases.

To test measurement feasibility of a 3D omnidirectional sensor in this study, a real indoor condition was simulated by using a 3D scene composed of different shapes; a cone and a triangular pyramid were used, as shown in Fig. 11. The captured image and the measured point cloud of the 3D scene are shown in (b) and (c); it can be observed that the 3D reconstruction of the point cloud matches well with the 3D profile of the measured object.

5. Conclusion

This paper aims to design a 3D omnidirectional sensor with high accuracy, high resolution, and large FOV. Through analysis of the defects in existing systems, we use scanning mirror to achieve a 3D omnidirectional sensing system with above advantages. Moreover, the combination of line laser and scanning mirror can prevent astigmatism phenomenon. The entire 3D ambient scene is achieved by a group of consecutive slices of point cloud of 3D profile. The reconstruction speed only depends on the frame rate of camera, which means real-time reconstruction can be achieved.

The developed 3D omnidirectional sensor consists of line laser transmitter and receiver and the geometrical relation is also studied in this paper. The prerequisite of accuracy measurement is to determine the optical plane of line laser beam; thus, the system calibration method is provided. A 3D omnidirectional sensor prototype is developed and constructed by the key components of a catadioptric camera, a rotating polygonal scanning mirror, and two line laser diodes. Several experiments were implemented and analyzed to verify accuracy and feasibility of the proposed 3D sensor.

Acknowledgment

The work is partially supported by National Science Foundation of China with Nos. 11102039 and 51105218 and the Fund of State Key Laboratory of Tribology of China (Grant no. SKLT2015B10).

References

[1] Nourbakhsh IR, Andre D, Tomasi C, Geneserech MR. Mobile robot obstacle avoidance via depth from focus. Robot Auton Syst 1997;22(2):151–8.
[2] Wang TQ, Chen QJ. Object semantic map representation for indoor mobile

robots. In: International conference on system science and engineering, Macao, China; June 8–10, 2011. p. 309–13.
[3] Khoshelham K, Elberink SO. Accuracy and resolution of kinect depth data forindoor mapping applications. Sensors 2012;12(2):1437–54.
[4] Henry P, Krainin M, Herbst E, Ren XF, Fox D. RGB-D mapping: using Kinect-style depth cameras for dense 3D modeling of indoor environments. Int J Robot Res 2012;31(5):647–63.
[5] Loreto S, Basilio S, Modesto C, Javier L, Maria MJ, Elena L. On the use of alow-cost thermal sensor to improve Kinect people detection in a mobile robot. Sensors 2013;13(11):14687–713.
[6] Biswas J, Veloso M. Depth camera based indoor mobile robot localization andnavigation. In: IEEE international conference on robotics and automation, Saint Paul, USA; May 14–18, 2012. p. 1697–1702.
[7] Rituerto A, Puig L, Guerrero JJ. Comparison of omnidirectional and conventional monocular systems for visual SLAM. In: The 10th workshop on omnidirectional vision, camera networks and non-classical cameras, Zaragoza, Spain; June 27, 2010. p. 1–13.
[8] Firoozfam P, Negahdaripour S. A multi-camera conical imaging system forrobust 3D motion estimation, positioning and mapping from UAVs. In: IEEE conference on advanced video and signal based surveillance, Miami, USA; July 21–22, 2003. p. 99–106.
[9] Benosman R, Kang SB. Panoramic vision: sensors, theory, and applications. New York: Springer; 2001.
[10] Neves AJR, Pinho AJ, Martins DA, Cunha Bernardo. An efficient omnidirectionalvision system for soccer robots: from calibration to object detection. Mechatronics 2011;21(2):399–410.
[11] Yi S, Choi B, Ahuja N. Real-time omnidirectional distance measurement withactive panoramic vision. Int J Control Autom Syst 2007;5(2):184–91.
[12] Yi S, Suh J, Hong Y, Hwang D. Active ranging system based on structured laserlight image. In: Proceedings of SICE annual conference, Taipei, China, August 18–21, 2010. p. 747–52.
[13] Matsui K, Yamashita A, Kaneko T. 3-D shape measurement of pipe by range finder constructed with omni-directional laser and omni-directional camera. In: IEEE international conference on robotics and automation, Anchorage, USA; May 3–7, 2010. p. 2537–42.
[14] Orghidan R, Salvi J, Mouaddib EM. Modelling and accuracy estimation of a new omnidirectional depth computation sensor. Pattern Recognit Lett 2006;27(7):843–53.
[15] Zhou FQ, Peng B, Cui Y, Wang YX, Tan HS. A novel laser vision sensor for omnidirectional 3D measurement. Optics Laser Technol 2013;45:1–12.
[16] Marino F, De Ruvo P, De Ruvo G, Nitti M, Stella E. HiPER 3-D: an omnidirectional sensor for high precision environmental 3-d reconstruction. IEEE Trans Ind Electron 2012;59(1):579–91.
[17] Ukida H, Yamato N, Tanimoto Y, Sano T, Yamamoto H. Omni-directional 3d measurement by hyperbolic mirror cameras and pattern projection. In: IEEE international instrumentation and measurement technology conference, Victoria, USA; May 12–15, 2008. p. 365–70.
[18] Zhang C, Xu J, Xi N, Jia YY, Li WX. Development of an omni-directional 3D camera for robot navigation. In: IEEE/ASME international conference on advanced intelligent mechatronics, Kaohsiung, China; July 11–14, 2012. p. 262–7.
[19] Benosman R, Kang SB. Panoramic vision: sensors, theory, applications.Germany: Springer Verlag; 2001.
[20] Scaramuzza D, Martinelli A, Siegwart R. A toolbox for easily calibrating omnidirectional cameras. In: IEEE/RSJ international conference on intelligent robots and systems; 2006. p. 5695–701.